Section 5

CORRECTIONS TO RAW CALORIMETER ENERGIES

Calorimeter information is used to estimate the jet momenta and the net transverse momentum of the particles recoiling against the $t\bar{t}$ system. This section details how those estimates are made. The signal from each calorimeter tower is converted into a raw [48] energy estimate. Tower energies are then used to evaluate the total energy in the event and other quantities used in the top mass analysis. The raw measurements are corrected for non-instrumented regions, non-linear response of the calorimeter, multiple interactions at high luminosity, and other effects, before a constrained fit is applied to the $t\bar{t}$ candidate events. Also in this section checks of the jet energy scale are discussed, this being the source of the largest systematic uncertainty in the measurement of the top quark mass.

5.1 Jet corrections and their uncertainties

The raw momentum of a jet is calculated by adding vectorially the momenta from all the towers belonging to the jet cluster (see Section 3.2).

Tower momenta are calculated from tower energies with the assumption that they are energies of particles with zero mass [49] that originate from the reconstructed primary vertex and are located at the center of the tower. To measure the top quark mass from candidate $t\bar{t}$ events, corrections are applied to the raw jet momenta in order to obtain estimates of the momenta of the daughter partons in the $t\bar{t}$ decay. The corrections occur in two stages.

- A set of "flavor-independent" corrections [33] is applied to all jets with raw $\mathrm{E_T} > 8$ GeV.
- A second set of corrections, specific to $t\bar{t}$ events, is applied to the leading four jets which are assumed to be the daughter jets from the $t\bar{t}$ decay. These corrections are applied after the flavor-independent corrections, and map the measured jet momenta to the momenta of the partons in the $t\bar{t}$ decay.

A description of the corrections to the raw jet momenta is the focus of this section.

5.1.1 Flavor-independent jet corrections

To account for detector and reconstruction effects, raw jet transverse momenta are corrected using a set of "flavor-independent" jet corrections [33]. The following expression includes all the corrections applied:

$$P_T(R) = (P_T^{raw}(R) \times f_{rel} - UEM(R)) \times f_{abs}(R) - UE(R) + OC(R). \quad (5.1)$$

The parameter $\mathrm{R}=\sqrt{(\Delta\eta)^2 + (\Delta\phi)^2}$ is the cone radius chosen for the jet measurement; R=0.4 for this analysis. The corrections are described below:

- f_{rel}, the relative energy scale, corrects for non-uniformities in calorimeter response as a function of η.

- $UEM(R)$ takes into account energy due to multiple interactions in the event.
- $f_{abs}(R)$, the absolute energy scale, maps the raw jet energy observed in a cone of radius R into the average true jet energy. This average is determined in the central calorimeter assuming a flat $\mathrm{P_T}$ spectrum.
- $UE(R)$ takes into account the energy due to the underlying event, i.e., the energy from the primary $p\bar{p}$ interaction due to fragmentation of partons not associated with the hard scattering,
- $OC(R)$, corrects for the energy expected to be outside the cone radius of 0.4.

The $f_{abs}(R)$ and the $OC(R)$ corrections are functions of the transverse momentum of the jet. The relative correction is primarily dependent on the pseudorapidity of the jet, with only a weak dependence on the jet momentum.

The reconstruction of jets starts with the raw clustered energy, $\mathrm{P_T}^{raw}(0.4)$. An uncertainty of $\pm 1\%$ is assigned to the stability of the calorimeter over the course of the data taking period. This systematic uncertainty was evaluated by comparing the response of the calorimeter to single charged tracks between data from Run 1 and data from the 1988–1989 run, which was used for the energy calibration discussed later. No systematic difference was observed. Also the raw inclusive jet cross section [50] obtained with the 1988-1989 data run was compared with that of the Run 1a data (after correcting for multiple interactions) and it was found that the ratio was consistent with unity at the 5% level. Because of the rapidly falling $\mathrm{E_T}$ spectrum, this corresponds to an upper limit on a difference in the energy scale of 1%.

The relative correction is derived from di-jet balancing data and corrects for the relative response of the different calorimeter sections to that of the calorimeter in the central region $(0.2 < |\eta| < 0.7)$ [49]. The plug

$\lvert\eta\rvert$ range	Uncertainty on relative correction
$0.0 - 0.1$	2.0 %
$0.1 - 1.0$	0.2 %
$1.0 - 1.4$	4.0 %
$1.4 - 2.2$	0.2 %
$2.2 - 2.6$	4.0 %
$2.6 - 3.4$	0.2 %

Table 5.1: The percentage uncertainty on the relative jet energy correction for various detector η ranges. The cracks in η between different detectors are located near η=0, 1.2, and 2.4, and have larger uncertainties than the regions away from the cracks.

($1.1 < |\eta| < 2.4$) and forward ($2.4 < |\eta| < 4.2$) regions are thus calibrated. The precision to which this calibration is known is limited mostly by the number of di-jet events available. The effects of different resolutions of the central and plug calorimeters on the energy measurements were studied using Monte Carlo simulation and are properly included. The uncertainty is larger near the cracks between the different detectors due to smaller statistics and worse energy resolution. Table 5.1 gives the uncertainty (in %) on the relative corrections for various detector η ranges.

The corrections for multiple interactions (UEM) in the same event and the underlying event (UE) in the primary interaction are derived from minimum bias data. The average number of interactions in Run 1a (N_v=0.6) is different from that of Run 1b (N_v=1.8), hence a different procedure is used for the two samples. For the Run 1a sample, 0.72 GeV/c is subtracted from the jet P_T after the absolute correction and accounts for both effects on average. For Run 1b, the effects of the underlying event and additional interactions are separated. To account for multiple interactions, prior to the absolute correction, 0.297 GeV/c is subtracted from the jet P_T for each additional reconstructed vertex in the event. This correction is obtained by studying the amount of energy in the event as a function of the number of vertices over the course of the run. For the underlying event (UE), we subtract 0.65 GeV/c from each jet after the absolute correction.

The uncertainty on the UEM correction is estimated to be 100 MeV/c for each vertex in the event. The uncertainty in the UE correction is evaluated by looking at variations in the energy density at $\pm 90^{\circ}$ with respect to the two jets in di-jet events when varying the maximal $\mathrm{E_T}$ threshold on the third jet from 5 to 15 GeV. Based on these studies, we assign a $\pm 30\%$ relative uncertainty to the underlying event correction [49, 33]. For jets with $\mathrm{P_T} > 20$ GeV/c the uncertainty is typically less than 0.5% of the jet's $\mathrm{P_T}$, as shown in Fig. 5.1.

The absolute correction is derived from data and Monte Carlo plus detector simulation. The simulation includes many features of the CDF calorimeters, the main ones being: non-linearity, cracks and less sensitive regions, single tower thresholds. The response of the calorimeter to incident pions and electrons is studied using testbeam data, minimum bias runs, special runs which triggered on events containing single isolated tracks, as well as standard data runs. The detector simulation has been tuned to agree with these data. The step from individual particle response to jets is achieved by tuning the Monte Carlo (ISAJET) fragmentation parameters to reproduce a number of distributions observed in di-jet data: number of charged particles, spectra and invariant mass of charged particles, and the ratio of charged to neutral energy [33]. The derived correction then accounts for non-linearity of the calorimeter, energy losses near the boundaries of different calorimeter wedges, response variation as a function of the position along the wedge and all the other effects included in the simulation. The absolute correction, $f_{abs}(0.4)$, as a function of corrected jet P_T, P_T^{cor}, is shown in Fig. 5.2(a).

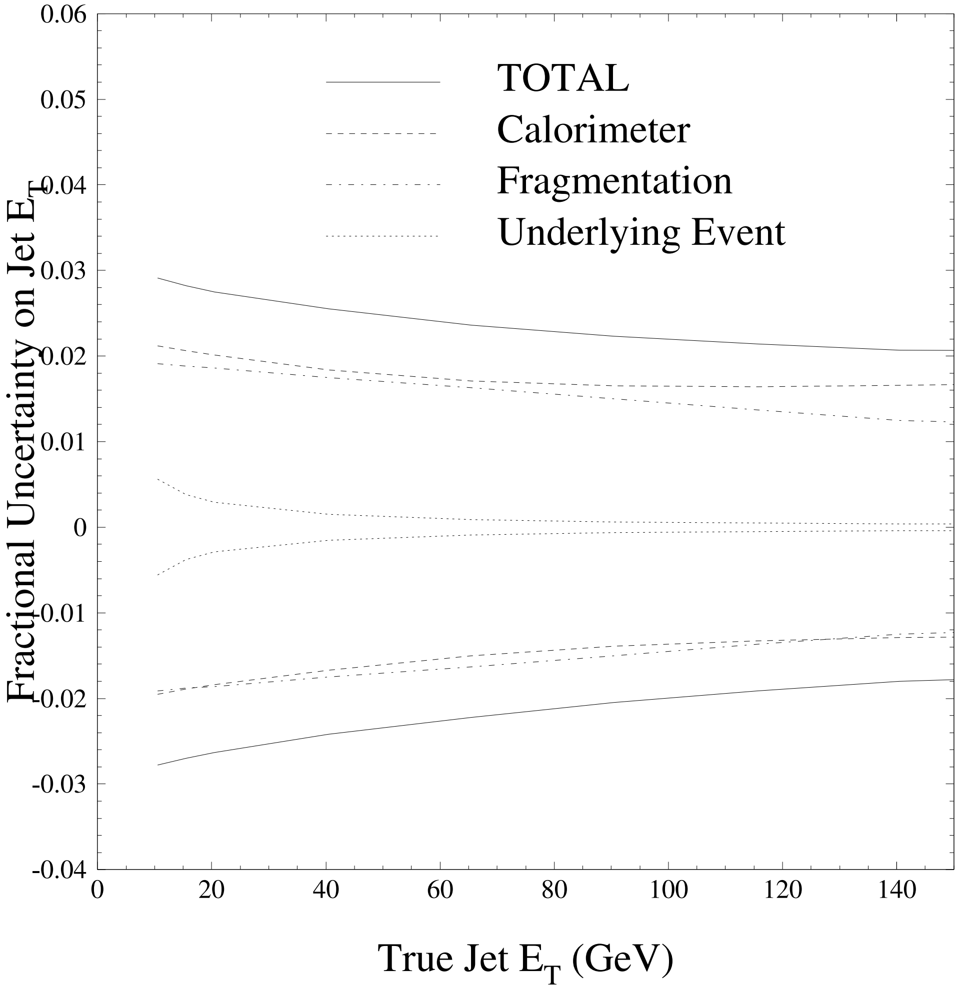

Figure 5.1: Uncertainty in jet E_T scale as measured with a jet clustering cone of size 0.4. The vertical axis shows the extent to which the measured jet E_T response varies due to different systematic effects.

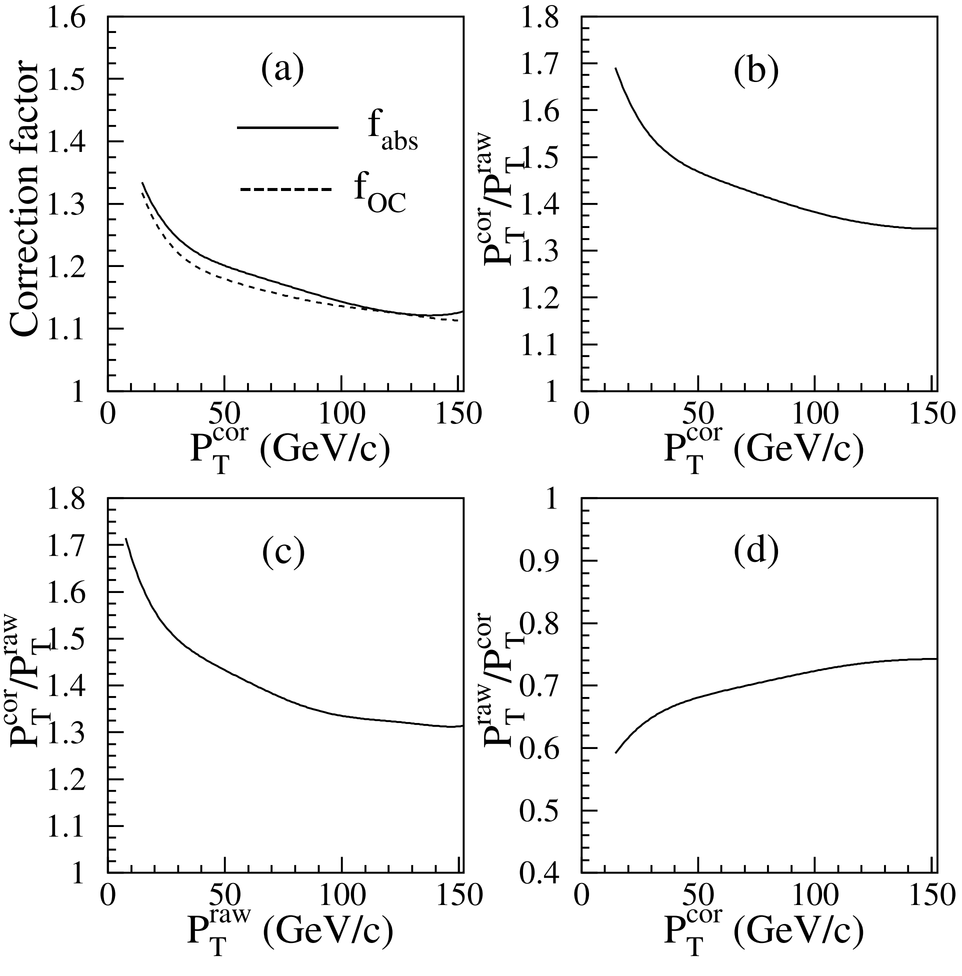

Figure 5.2: "Flavor-independent" jet corrections, for a jet clustering cone of R=0.4. (a) Absolute correction, f_{abs}, and out-of-cone correction factor, $1+\mathrm{OC}/\mathrm{P_T}$, versus corrected jet $\mathrm{P_T}$, $\mathrm{P_T^{cor}}$. (b) Total correction, $\mathrm{P_T^{cor}}/\mathrm{P_T^{raw}}$, as a function of $\mathrm{P_T^{cor}}$. (c) total correction, $\mathrm{P_T^{cor}}/\mathrm{P_T^{raw}}$, as a function of $\mathrm{P_T^{raw}}$. (d) fraction of measured momentum, $\mathrm{P_T^{raw}}/\mathrm{P_T^{cor}}$ versus $\mathrm{P_T^{cor}}$.

The systematic uncertainty in the absolute correction is attributed to (a) calorimeter response, and (b) fragmentation related effects [49, 33] (see Fig. 5.1). The parameters that describe the calorimeter's response to incident electrons, photons and pions have uncertainties due to finite statistics and assumptions which are made. For example, at low momentum ($|p| < 5$ GeV/c), the largest source of uncertainty in the charged pion response comes from the estimation of the amount of energy in the shower from π^0's. Additional uncertainty comes from the uncertainty in the relative response across the face of a calorimeter cell and the energy deposition in cracks between calorimeter cells. The uncertainty in the calorimeter's response to photons is assigned to be the same as for electrons. Uncertainty in the fragmentation parameters comes from the modeling of the tracking efficiency in jets, and the level of agreement between the simulation and data.

The contributions to the jet E_T uncertainty from these sources are evaluated by shifting the input values of these parameters by $+1$ and -1 standard deviation ($+1\sigma$ and -1σ), and calculating the resulting shift in the reconstructed jet energies. For (a) we separately vary the pion, electron, and photon responses by $+1\sigma$ and -1σ, and add the resulting shifts in the jet energies in quadrature. For (b), we vary the charged tracking efficiency by its uncertainty and reevaluate a new set of fragmentation parameters. These new fragmentation parameters are in turn varied one at a time, and the resulting deviations in the jet energies are added in quadrature.

The systematic uncertainties in the jet E_T scale from the sources (a) and (b), as well as from the UE correction are shown in Fig. 5.1. The total systematic uncertainty from these three sources is obtained by adding in quadrature the three curves, and is shown as the solid curve in Fig. 5.1.

The out-of-cone correction was derived from a Monte Carlo simulation and accounts for the energy falling outside the jet cone [49]. This study was done with light quarks; the $t\bar{t}$ specific corrections take into account differences with heavy flavor jets. The amount of energy outside the cone of R=0.4 is related to emission of low energy gluons from the initial partons, and is referred to as "soft gluon" radiation. The correction factor, $f_{OC} = 1+OC(0.4)/\mathrm{P_T}(0.4)$, is a function of the jet $\mathrm{P_T}$ corrected for all other effects and is given by the equation,

$$f_{OC} \;=\; 1.0 + \frac{23.0\,(1.0 - 0.915\,e^{-0.0074\,\mathrm{P_T}})}{\mathrm{P_T}}. \tag{5.2}$$

The correction factor is shown in Fig. 5.2(a).

The systematic uncertainty on the jet momentum from the OC correction originates from the uncertainty in modeling the radiation of low energy gluons in parton showers. To estimate this uncertainty, we use W+1 jet data and a HERWIG Monte Carlo simulation of W+1 jet events to compare the energy contained in an annulus with radii of 0.4 and 1.0 around the jet direction. We define a variable F,

$$F \;=\; \frac{\mathrm{P_T}(1.0) - \mathrm{P_T}(0.4)}{\mathrm{P_T}(0.4)} \tag{5.3}$$

where $\mathrm{P_T}(0.4)$ and $\mathrm{P_T}(1.0)$ are the jet momenta corrected using the corrections described above (note that Eq. 5.2 is used for R=0.4; for R=1.0 the correction is much smaller). The quantity F is the fractional difference of the momentum in an annulus with radii between 0.4 and 1.0, calculated for each event using the calorimeter towers in that annulus or using the average OC correction. A comparison of data and Monte Carlo tests the agreement between the Monte Carlo soft gluon radiation modeling and what is observed in the data in that annulus. Figure 5.3 shows the mean value of F as a function of the corrected $\mathrm{P_T}$ (corrected using a cone size of 0.4) for data and Monte Carlo. There is a clear difference between the two distributions. This implies that the jet shapes in data and Monte Carlo disagree at the few % level. The difference between HERWIG and data is shown in Fig. 5.4. We take this difference as the uncertainty on the out-of-cone correction. Its effect on the top quark mass measurement is referred to as the systematic uncertainty from soft gluon radiation.

Similar distributions have been obtained for other sets of data, namely $Z+1$ jet data and jet data with two b-tagged jets. Since the statistics for the latter sets of data are low, only the $W+1$ jet data are used. A fit to the points of Fig. 5.4 gives a maximum (upper dotted curve) uncertainty of $\delta\mathrm{P_T}/\mathrm{P_T} = \exp(2.467 - 0.074\mathrm{P_T}) + 1.438$ (in %). It can be seen that for jets typical of those produced in $t\bar{t}$ events ($\approx 30-90$ GeV for $M_{top} = 175$ GeV$/c^2$), the difference between HERWIG and data is $< 2\%$. For softer jets, the difference is closer to 4%.

The systematic uncertainty assigned to the soft gluon radiation accounts for differences in the energy contained in the annulus $0.4 < R < 1.0$ between data and the Monte Carlo simulation. For the additional energy which falls outside a cone of 1.0, we assign an uncertainty of $\pm$ 1 GeV. We refer to this energy as "splash-out".

In summary, Figure 5.2 shows some of the flavor-independent jet corrections and their $\mathrm{P_T}$ dependence. Figure 5.2(a) shows the absolute and out-of-cone correction factors as a function of the corrected jet $\mathrm{P_T}$. They vary from $\approx$1.3 at $\mathrm{P_T} = 15$ GeV$/c$ to $\approx$1.12 for $\mathrm{P_T} > 100$ GeV$/c$. Figure 5.2(b) shows the ratio of the fully corrected jet $\mathrm{P_T}$ ($\mathrm{P_T^{cor}}$) to the raw jet $\mathrm{P_T}$ ($\mathrm{P_T^{raw}}$) as a function of the fully corrected jet $\mathrm{P_T}$. Jets from $t\bar{t}$ events typically have a $\mathrm{P_T}$ of $\approx 30-90$ GeV$/c$, for which the average jet correction factor is $\approx$ 1.45. Figure 5.2(c) shows the correction factor as a function of $\mathrm{P_T^{raw}}$. Finally, Fig. 5.2(d) shows the fraction of momentum measured in the detector before the jet corrections as a function of the corrected jet $\mathrm{P_T}$. Figure 5.5 shows the overall systematic uncertainty as a function of the corrected $\mathrm{P_T}$ of the jets. In the 30-90 GeV$/c$ range, the systematic uncertainty on jet energies is about 4%.

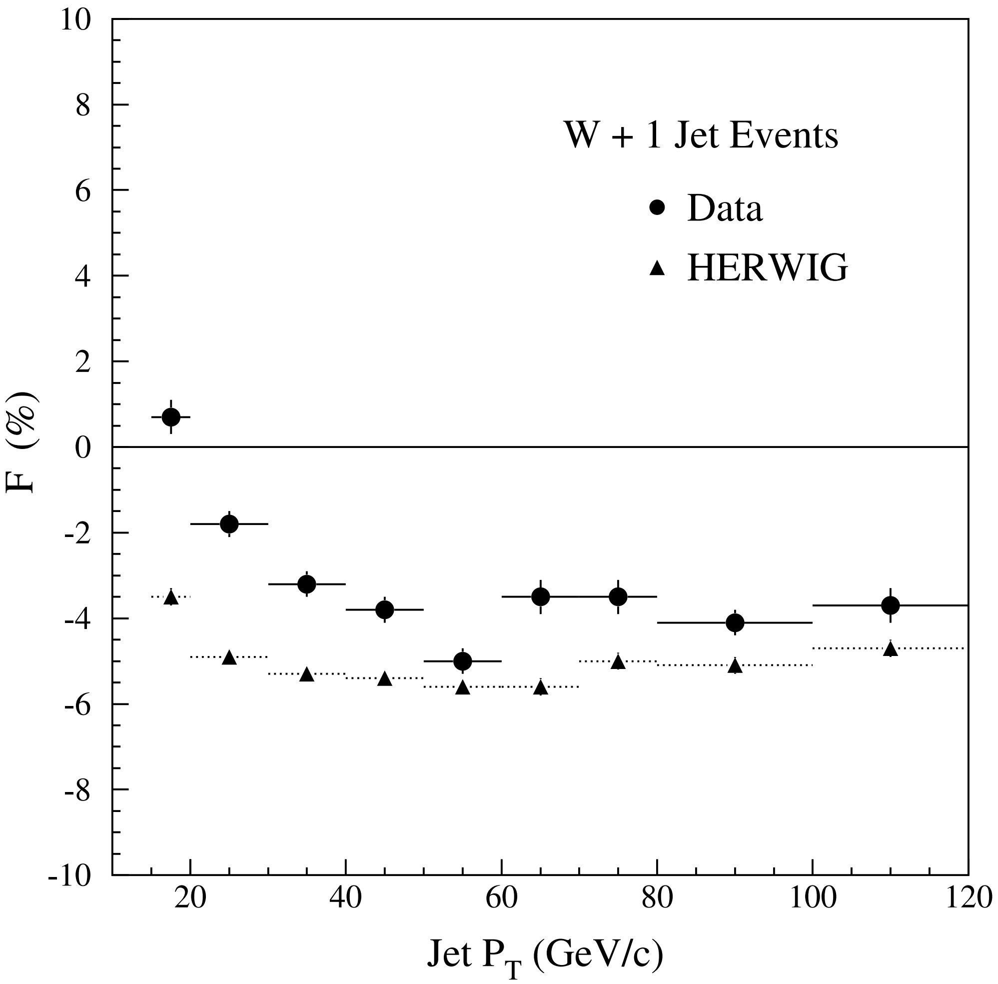

Figure 5.3: Fractional difference in corrected jet P_T obtained using cone radii of 0.4 and 1.0 as a function of the corrected jet P_T from W+1 jet events. The circles are the results from the data sample and the triangles are from a sample of HERWIG Monte Carlo events which have been processed through the CDF detector simulation.

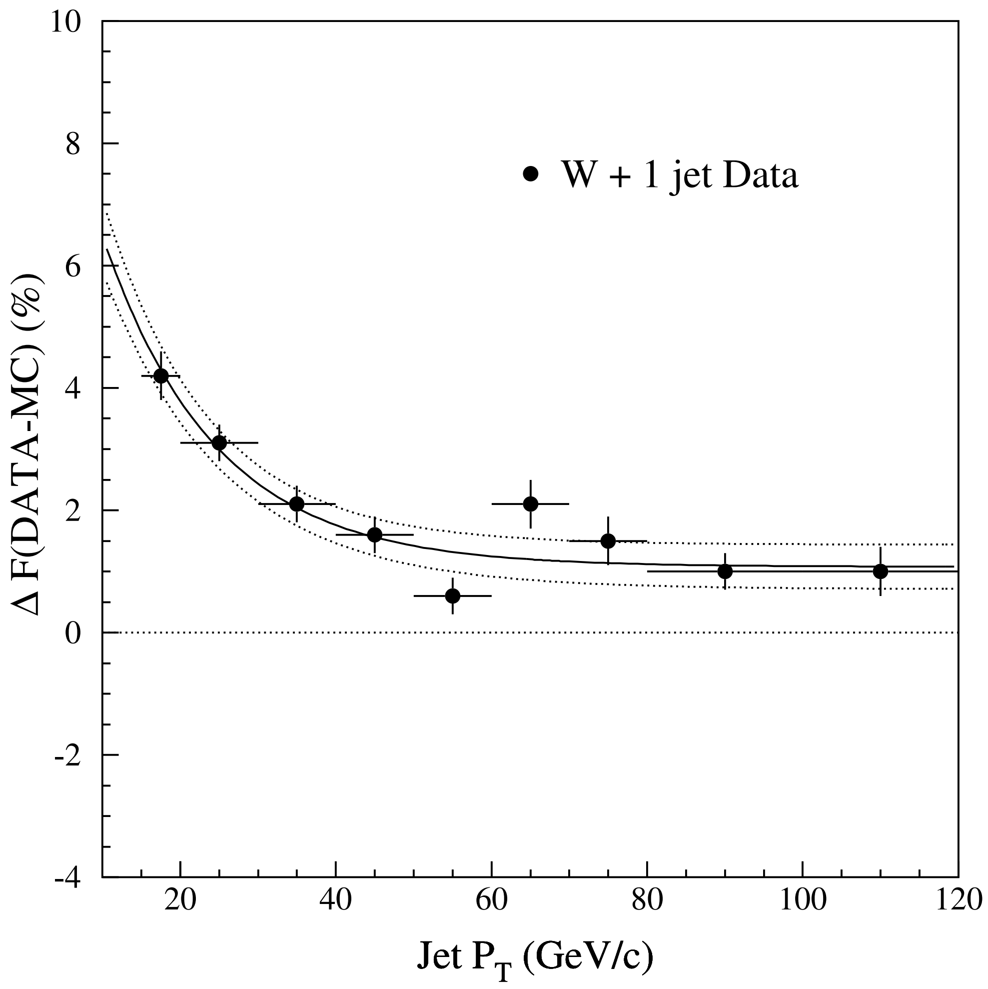

Figure 5.4: Systematic uncertainty on the out-of-cone correction as obtained in W+1 jet events. The abscissa is the fully corrected jet P_T using a clustering cone of 0.4. The vertical axis is the difference between data and Monte Carlo of the variable F described in the text. The full curve represents a fit through the data points, the dotted curves were obtained using the one standard deviation values of the fit parameters.

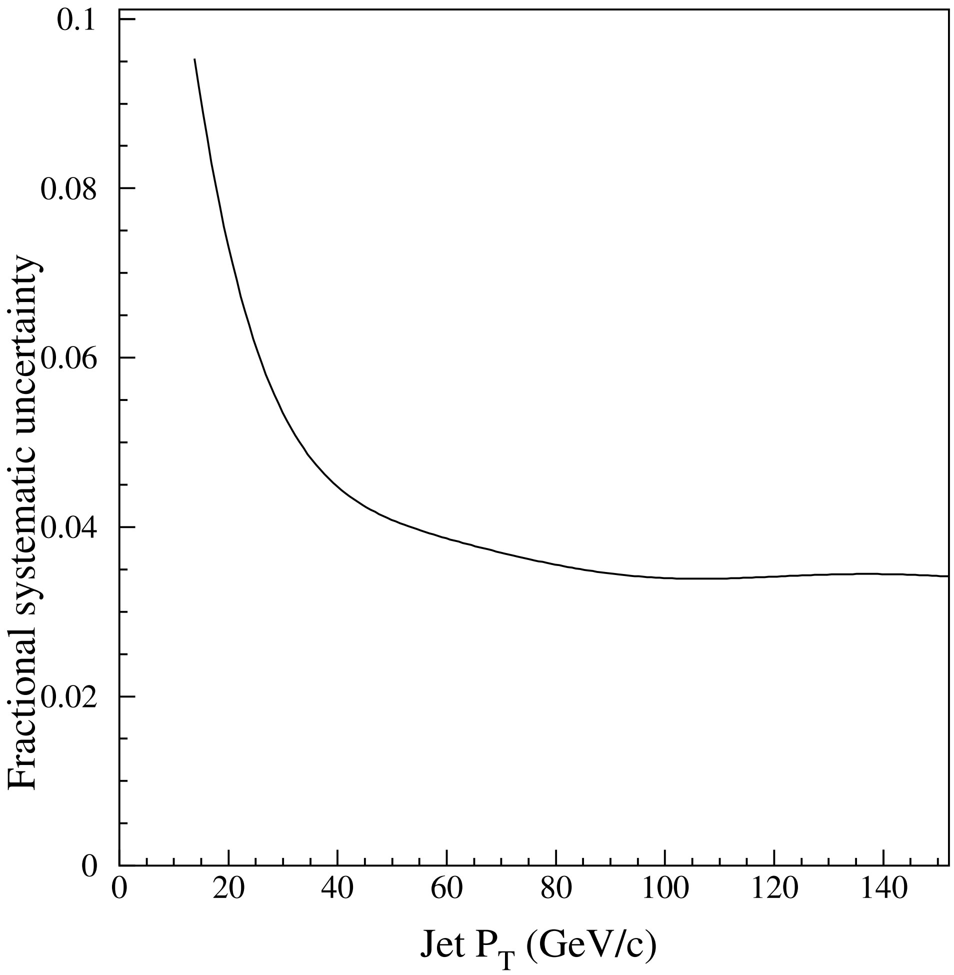

Figure 5.5: Total systematic uncertainty on jets as a function of the corrected jet P_T.

5.1.2 Checks on the jet E_T scale and its uncertainty

The procedures used to obtain the jet corrections and their systematics have been checked by applying them to $Z + 1$ jet events, where the Z-boson decays into either e^+e^- or $\mu^+\mu^-$. The energy scale for electrons and the momentum scale for muons are known to a precision of 0.14% and 0.065% respectively [31]. In the absence of initial state radiation, such events are expected to have zero net transverse momentum. The jet in each event is corrected according to the previous prescription, and the quantity

$$F_b = \frac{\mathrm{P_T}(Z) - \mathrm{P_T}(\mathrm{jet})}{\mathrm{P_T}(Z)} \tag{5.4}$$

is calculated, where $\mathrm{P_T}(Z)$ is in the range 30-150 GeV/c. The lower limit was chosen to avoid biases due to the sample selection. The jet recoiling against the Z boson is required to have an uncorrected $\mathrm{E_T} \geq 8$ GeV and $|\eta| < 2.4$. To test the jet energy scale we need a clean environment, i.e., events in which there is only one jet recoiling against the Z boson. We therefore require that any additional calorimeter cluster have an uncorrected energy $\mathrm{E_T} < 6.0$ GeV (at any η).

To separate detector effects from those due to gluon radiation in the initial state, we use the component analysis first suggested in Ref [51]. We compute the direction of the bisector between the Z and the jet directions in the transverse plane. The "parallel component" of F_b is then defined to be the component perpendicular to the bisector. Balancing the jet against the Z along this component will give information about the jet energy scale. Figure 5.6 shows the distribution of this component of F_b in $Z+1$ jet events for data and Monte Carlo. The difference in the medians of the two distributions is:

$$(\Delta F_b)_{||} = (3.2 \pm 1.5(stat) \pm 4.1(syst))\%. \tag{5.5}$$

The 4.1% systematic uncertainty was calculated using the jet energy uncertainties discussed in the previous section. We conclude that any possible energy scale shift detected by this check is compatible with zero within the evaluated uncertainties.

5.1.3 Jet momentum corrections for $t\bar{t}$ events

The $t\bar{t}$ specific jet momentum corrections are designed to make an average correction to the jet momenta to obtain an estimate of the original parton momenta [1]. The $\mathrm{P_T}$ spectra of partons from HERWIG generated $t\bar{t}$ events which pass our experimental selection cuts are shown in Fig. 5.7. The $t\bar{t}$-specific corrections account for (a) the difference in the $\mathrm{P_T}$ spectrum between top induced jets and the flat spectrum used to derive the flavor-independent corrections, (b) the energy lost through semileptonic b and c-hadron decays, and (c) the multi-jet final state of $t\bar{t}$ events as compared to di-jet final state used to derive the flavor-independent corrections. The correction for these three effects are derived using the HERWIG Monte Carlo generator with an input top quark mass of 170 GeV/c^2. The generated events are processed using the CDF simulation and reconstructed in the same way as the data sample. An average correction factor is determined by first matching (in $\eta-\phi$ space) the reconstructed jets with the generated partons, and then comparing the reconstructed jet P_T (after the flavor-independent corrections) with the original parton P_T. The correction is given by the median of the distribution of $\Delta = (\mathrm{P_T}(parton) - \mathrm{P_T}(jet))/\mathrm{P_T}(jet)$. This is done as a function of the reconstructed jet $\mathrm{P_T}$.

Figure 5.8 shows the size of the $t\bar{t}$-specific correction factors for four types of jets: (A) jets from hadronic W decays, (B) average b jets (no selection on decay mode) (C) b jets containing an electron, and (D) b jets containing a muon. The general shape of each curve is primarily a result of the difference between using a flat jet $\mathrm{P_T}$ spectrum and the spectrum appropriate for top decays. In particular, this difference is responsible for the rising values of the curves at low $\mathrm{P_T}$, and the asymptotic values at large $\mathrm{P_T}$. The larger

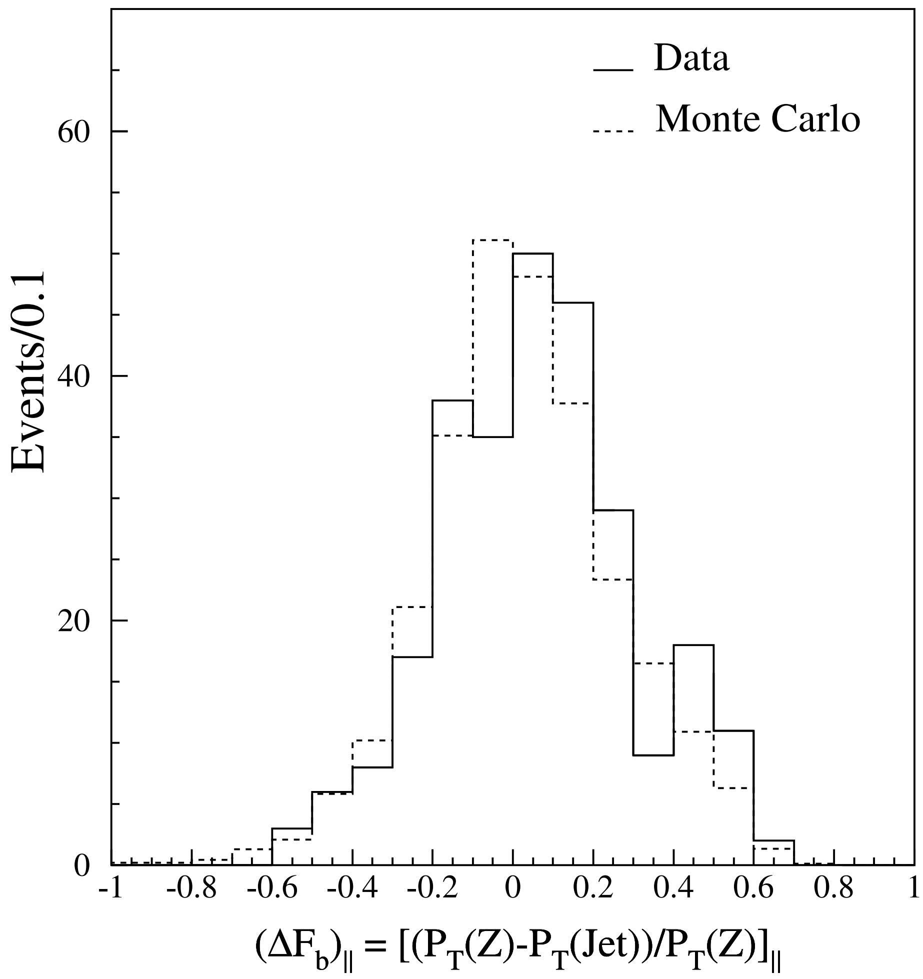

Figure 5.6: Parallel component of transverse momentum imbalance between the Z and the jet in reconstructed $Z+1$ jet candidate events. Both data (solid) and Monte Carlo (dashed) are shown (see text).

corrections applied to the b jets with a soft lepton are a consequence of the amount of energy carried off by undetected neutrinos, and, for jets containing a $b \to \mu\nu X$ decay, of the fact that muons deposit only $\approx$2 GeV, on average, in the calorimeter.

The flavor-independent and $t\bar{t}$-specific corrections bring the median reconstructed jet $\mathrm{P_T}$ into agreement with the initial parton $\mathrm{P_T}$ in $t\bar{t}$ events. The uncertainty on the jet $\mathrm{P_T}$ after these corrections is given by the σ of the Δ distribution, defined as one half of the separation of the 16th and 84th percentiles of the distribution. For each bin of reconstructed jet $\mathrm{P_T}$, we obtain the σ of the Δ distribution, which is then parametrized as a function of the reconstructed jet $\mathrm{P_T}$. These uncertainties are shown in Fig. 5.9 for jets from W decay and b jets. As above, we display curves for generic b jets (no selection on decay mode), for jets containing an electron, and for jets containing a muon. These jet $\mathrm{P_T}$ uncertainties are input into the kinematic mass fitter (see Section 6) and dictate how much the jet energies can be altered to accommodate the applied constraints.

The jet corrections described above are applied only to the four highest $\mathrm{P_T}$ jets in the event, which are assumed to be daughters of the t and $\bar{t}$ decays. Any additional jets beyond the leading four jets are corrected only with the "flavor-independent" corrections (excluding the out-of-cone corrections, see Section 5.2) and are assigned an uncertainty of $0.1\mathrm{P_T} \oplus 1$ GeV/c. This curve is also shown in Fig. 5.9.

5.1.4 Summary of systematic uncertainties on jet energy measurements

A number of corrections are performed to estimate the original parton momenta from the observed jets. The jet energy scale uncertainty is evaluated from the uncertainties in the corrections for calorimeter stability, multiple

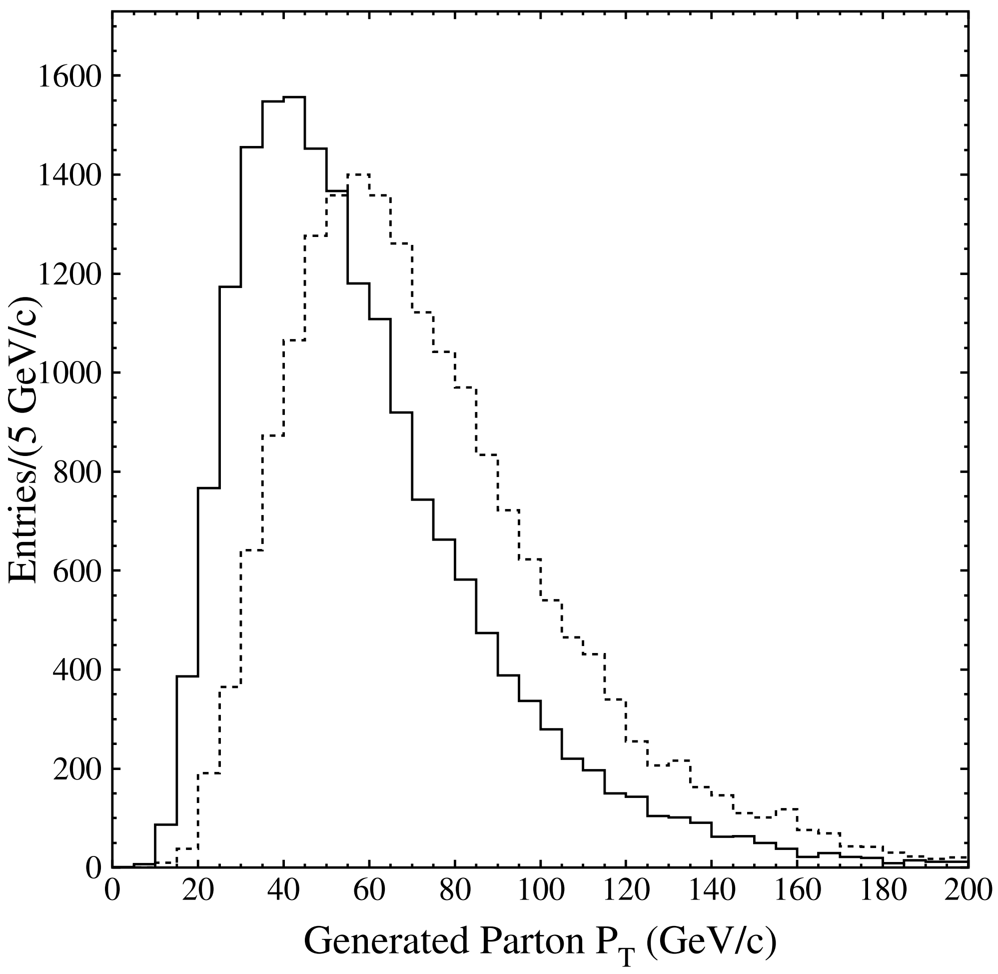

Figure 5.7: P_T distributions for partons from top quark decays obtained from the HERWIG Monte Carlo program after simulation of detector response and including the effects of the Top Mass Candidate Sample data selection. The solid line indicates the distribution for light quarks from the $W \to q\bar{q}'$ decay and the dashed line is the distribution for b quarks.

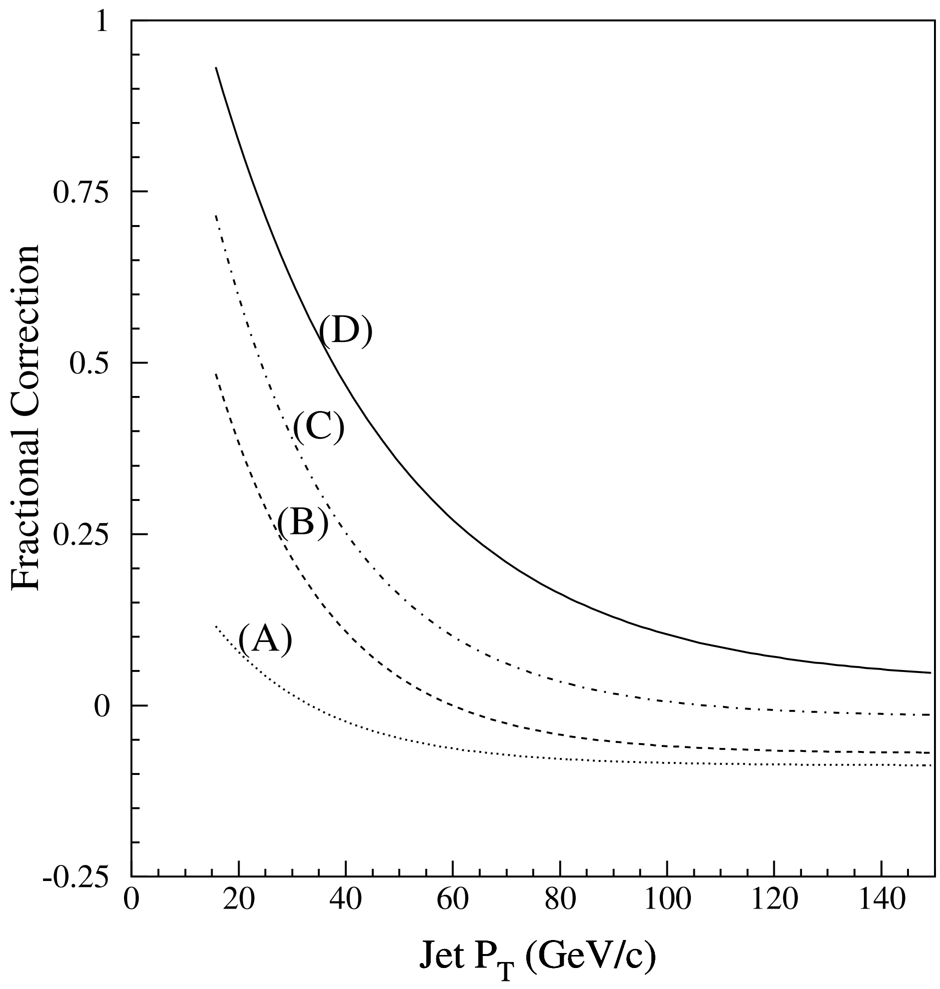

Figure 5.8: The $t\bar{t}$-specific corrections applied to jets according to available b-jet information. The curves show the fractional change to the corrected jet P_T after all "flavor-independent" jet corrections have been applied. The curves are for: (A) jets from the decay of W bosons, (B) jets from all b quarks (no selection on decay mode), (C) jets from b quarks containing an electron, and (D) jets from b quarks containing a muon.

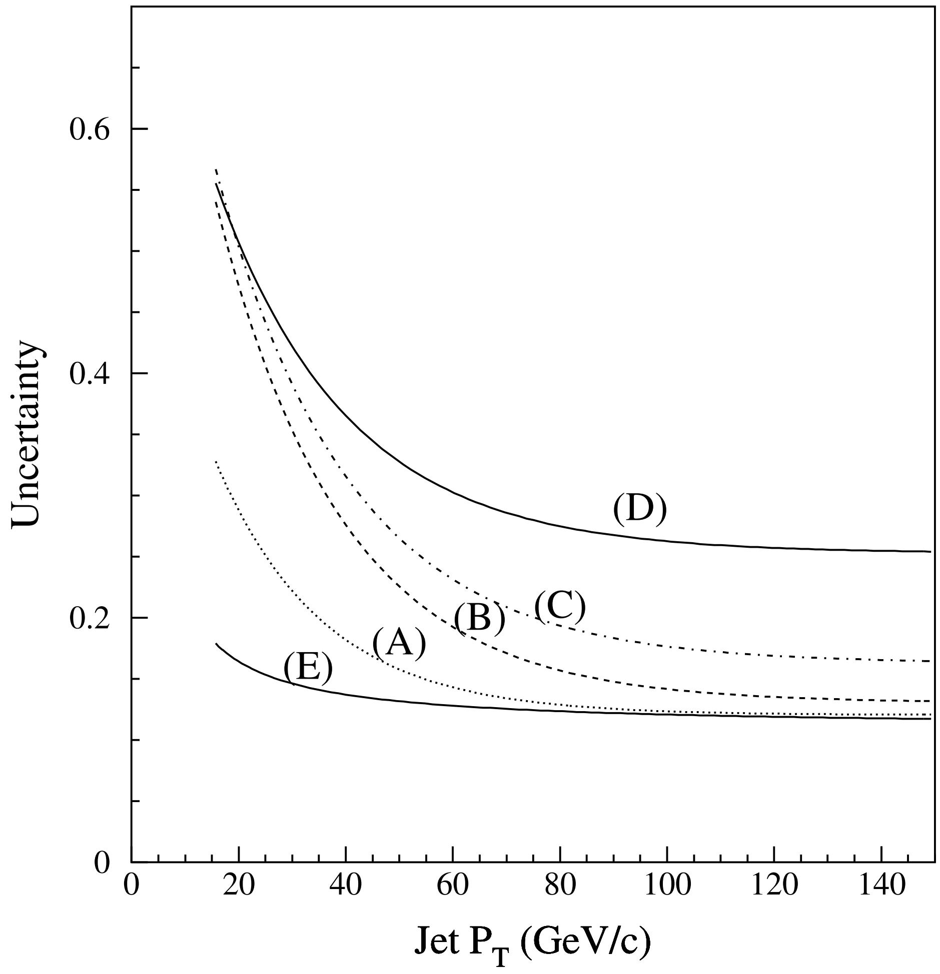

Figure 5.9: Fractional uncertainty in the estimated parton P_T as a function of the jet P_T after the flavor-independent jet corrections are applied. The uncertainty shown on the vertical axis is given as a fraction of the jet P_T. Curves (A) through (D) have the same meaning as for the previous figure. The curve labeled (E) is used for the jets beyond the four highest-P_T jets and is applied only to the P_T within the cone of radius R=0.4.

interactions, calorimeter response, jet fragmentation, underlying event, out-of-cone correction, and splash out. Figure 5.5 shows the dependence of the overall jet energy scale uncertainty on the corrected jet $\mathrm{P_T}$. The total systematic uncertainty varies between 7% for jets with corrected $\mathrm{P_T}$ of 20 GeV/c and 3.5% for jets with $\mathrm{P_T}$=150 GeV/c.

We do not assign a separate systematic uncertainty to the top specific corrections. Such uncertainties may arise from modeling of initial and final state gluon radiation, and modeling of the primary parton collision. We discuss these uncertainties in Section 9.

5.2 Measurement of other calorimeter variables

To measure the top mass we apply energy-momentum conservation to the process $p\bar{p} \to t\bar{t} + X$, with subsequent decay of the t ($\bar{t}$) into $W + b$ ($\bar{b}$) (see Section 6). Here, X is the unspecified particles which recoil against the $t\bar{t}$ system. The calorimeter provides the measurement of X_T, the transverse momentum of X. The quantity X_T is computed from the energy left over after the lepton and the four jets from the $t\bar{t}$ system are removed from the total measured energy. This leaves two terms:

$$\vec{X}_T = \vec{U}_T + \sum_{i=5}^{N_{jets}} \vec{E}_T(jet) \tag{5.6}$$

Each component of the unclustered energy, $\vec{U}_T$, is defined as the vector sum of the energies in the calorimeter towers after excluding the primary lepton and all the jets with raw $\mathrm{E_T} > 8$ GeV and $|\eta| < 3.4$ in the event. Using a $t\bar{t}$ Monte Carlo (M_{top} =175 GeV/c^2) we find a distribution in U_x with $\langle U_x \rangle \sim 0$ and $\sigma = 15.8$ GeV for events which enter into the mass subsamples. The same distribution for the data has a mean consistent with 0 and a $\sigma = 14.9$ GeV. The Monte Carlo and data distributions in U_x are shown in Fig. 5.10. Similar results are obtained for the y component.

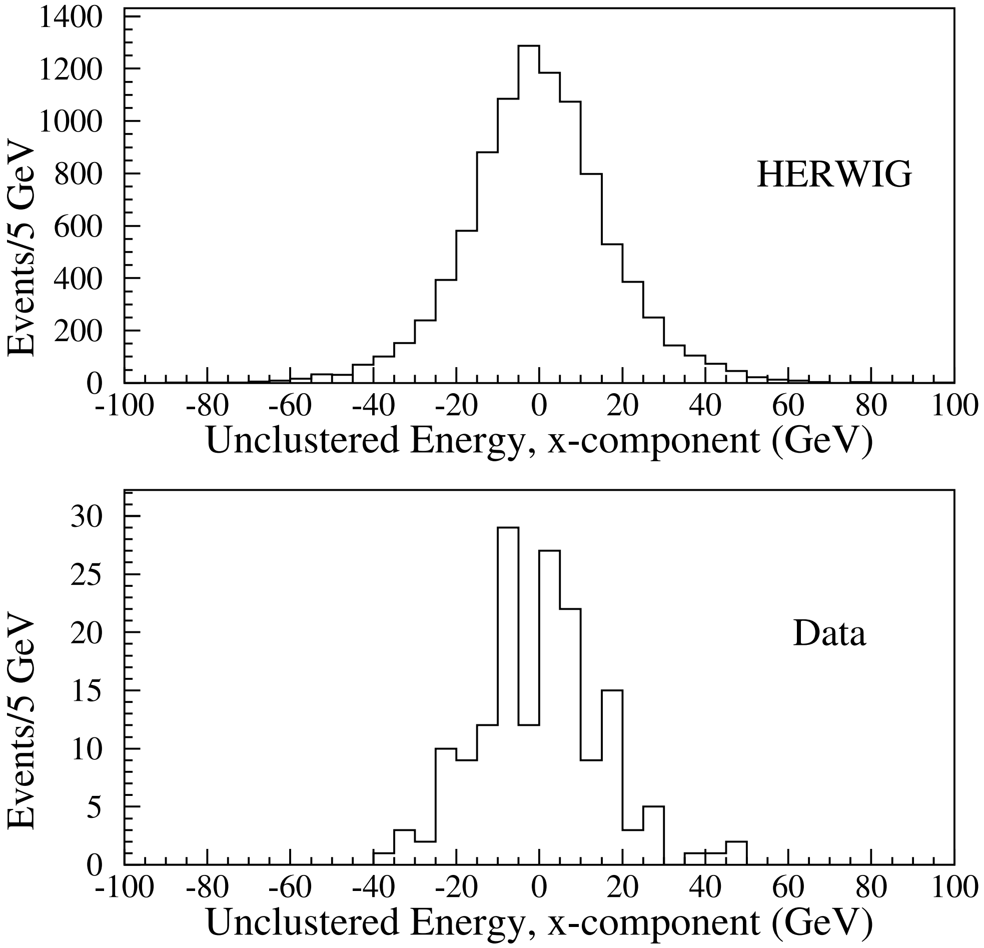

Figure 5.10: Unclustered energy for the mass sample used here and for $t\bar{t}$ Monte Carlo (M_{top} =175 GeV/c^2). Only the x component is shown.

Each component of the unclustered energy is corrected with a single factor $f_{u.e.} = 1.6$, based on studies of the recoil energy that the calorimeter measures in Z-boson events with no extra jets, where the Z boson is well measured by the two leptons it decays into [52]. The final mass value is not sensitive to the value of $f_{u.e.}$. For example, using $f_{u.e.} = 2.0$ makes a negligible change in the reconstructed top quark mass (0.2 GeV/c^2), hence it is not included in the Table of systematics in Section 9.7. The uncertainty with which each component of $\vec{U}_T$ is measured is taken to be 100% (added in quadrature to 1 GeV). The jets beyond the four with the highest $\mathrm{E_T}$ are corrected only within the cone of 0.4, so as to avoid counting the out of cone energy twice (it is already included in the unclustered energy). The uncertainties on these jet energies were discussed in Section 5.1.3 and shown in Figure 5.9.

Another quantity that can be estimated from the calorimeter measurement is the $\not{E}_\mathrm{T}$. It is calculated using the following expression:

$$-\vec{\not{E}}_T = \vec{E}_T(lepton) + \sum_{i=1}^{4} \vec{E}_T(jet) + \vec{X}_T \tag{5.7}$$

The above expression shows that the $\not{E}_\mathrm{T}$ measurement is highly correlated with the jet energy measurements, and therefore it is not considered as an independent measurement in the mass fitting. As discussed in Section 6, it is only used as a starting value for the neutrino's transverse momentum when the overall mass fit is performed.

REFERENCES

[1] F. Abe *et al.,* Phys. Rev. D **50**, 2966 (1994); Phys. Rev. Lett. **73**, 225 (1994).

[2] F. Abe *et al.,* Phys. Rev. Lett. **74**, 2626 (1995).

[3] S. Abachi *et al.,* Phys. Rev. Lett. **74**, 2632 (1995).

[4] F. Abe *et al.,* Phys. Rev. Lett. **75**, 3997 (1995); F. Abe *et al.,* Phys. Rev. D. **51**, 4623 (1995).

[5] S. Abachi *et al.,* Phys. Rev. Lett. **79**, 1197 (1997).

[6] F. Abe *et al.,* Phys. Rev. Lett. **80**, 2767 (1998).

[7] F. Abe *et al.,* Phys. Rev. Lett. **80**, 2773 (1998).

[8] S. Abachi *et al.,* Phys. Rev. Lett. **79**, 1203 (1997).

[9] F. Abe *et al.,* Phys. Rev. D. **59**, 092001 (1999).

[10] F. Abe *et al.,* Phys. Rev. Lett. **79**, 1992 (1997).

[11] B. Abbott *et al.*, Phys. Rev. Lett. **83**, 1908 (1999); Phys. Rev. D **60**, 012001 (1999).

[12] F. Abe *et al.,* Phys. Rev. Lett. **80**, 2779 (1998).

[13] B. Abbott *et al.,* Phys. Rev. Lett. **80**, 2063 (1998).

[14] M. Jezabek and J.H. Kuhn, Phys. Rev. D **48**, 1910 (1993); Erratum, *ibid.* **49**, 4970 (1994).

[15] I.I. Bigi, Yu L. Dokshitzer, V.A. Khoze, J.H. Kuhn, and P. Zerwas, Phys. Lett. B **181**, 157 (1986).

[16] S.L. Glashow, Nucl. Phys. **22**, 579 (1961); S. Weinberg, Phys. Rev. Lett. **19**, 1264 (1967); A. Salam, in *Elementary Particle Theory: Relativistic Groups and Analyticity (Nobel Symposium No. 8)*, edited by N. Svartholm (Almqvist and Wiksell, Sweden, 1968), p. 367.

[17] The LEP Collaborations, the LEP Electroweak Working Group and the SLD Heavy Flavor and Electroweak Groups, CERN-EP/99-15 (1999).

[18] F. Abe *et al.,* Phys. Rev. Lett. **79**, 3835 (1997).

[19] F.Abe *et al.,* Nucl. Instrum. Methods **A271**, 387 (1988).

[20] F. Bedeschi *et al.,* Nucl. Instrum. Methods **A268**, 50 (1988).

[21] The pseudo-rapidity η is defined as $-\log(\tan(\theta/2))$, where θ is the polar angle measured relative to the positive z-axis (taken as the direction of the outgoing proton beam) assuming a z-vertex position of zero. For the mass fit discussed in Section 6 we recalculate η using the measured z-vertex position for each event.

[22] F. Snider *et al.,* Nucl. Instrum. Methods **A268**, 75 (1988). This is the reference for the previous generation of the device. The replacement for the Run 1 data sample has more modules, each with a shorter drift length but is otherwise similar.

[23] F. Abe *et al.*, Phys. Rev. Lett. **76**, 3070 (1996).

[24] P. Azzi *et al.*, Nucl. Instrum. Methods **A360**, 137-140 (1995), for Run 1b. D. Amidei *et al.,* Nucl. Instrum. Methods **A350**, 73-130 (1994); D.

Amidei *et al.,* Nucl. Instrum. Methods **A342**, 251-259 (1994); C. Haber *et al.,* Nucl. Instrum. Methods **A289**, 388 (1990); for Run 1a.

[25] G. Ascoli *et al.,* Nucl. Instrum. Methods **A268**, 33 (1988); G. Ascoli *et al.,* Nucl. Instrum. Methods **A268**, 41 (1988).

[26] L. Balka *et al.,* Nucl. Instrum. Methods **A267**, 272 (1988); S. R. Hahn *et al.,* Nucl. Instrum. Methods **A267**, 351 (1988); K. Yasuoka *et al.,* Nucl. Instrum. Methods **A267**, 315 (1988); R. G. Wagner *et al.,* Nucl. Instrum. Methods **A330**, 272 (1988); T. Devlin *et al.,* Nucl. Instrum. Methods **A267**, 24 (1988).

[27] S. Bertolucci *et al.,* Nucl. Instrum. Methods **A267**, 301 (1988).

[28] The unclustered energy consists of the total energy which is not contained in jets with $\mathrm{E_T} > 8$ GeV and $|\eta| < 3.4$.

[29] The missing $\mathrm{E_T}$, $\not\!\!E_{\mathrm{T}}$ is defined to be the magnitude of the vector sum of the raw transverse energies in all calorimeter towers with $|\eta| < 3.6$. Only towers which exceed a detector-dependent energy threshold are included in the sum [1].

[30] A fiducial lepton is required to be within a well-understood region of the CEM which allows for good lepton identification.

[31] F. Abe *et al.,* Phys. Rev. D **52**, 4784 (1995); F. Abe *et al.,* Phys. Rev. Lett. **75**, 11 (1995).

[32] The isolation, I, is defined as the $\mathrm{E_T}$ ($\mathrm{P_T}$) within a cone of $\Delta R < 0.4$ centered on the lepton, but excluding the lepton energy, divided by the $\mathrm{E_T}$ ($\mathrm{P_T}$) of the lepton.

[33] F. Abe *et al.,* Phys. Rev. D **45**, 1448 (1992).

[34] D. Kestenbaum, Ph.D. Thesis (unpublished), Harvard University (1996).

[35] F. Abe *et al.,* Phys. Rev. Lett. **73**, 2662 (1994).

[36] K. Tollefson, Ph.D. Thesis (unpublished), University of Rochester (1997).

[37] A.D. Martin, R.G. Roberts, and W.J. Stirling, Phys. Lett. B **306**, 145 (1993).

[38] P. Avery, K. Read, G. Trahern, Cornell Internal Note CSN-212, March 25, 1985 (unpublished). We use Version 9_1 with a b lifetime of 1.45 ps.

[39] G. Marchesini and B.R. Webber, Nucl. Phys. **B310**, 461 (1988); G. Marchesini *et al.,* Comput. Phys. Comm. **67**, 465 (1992).

[40] T. Sjöstrand, Computer Physics Commun. **39**, 347 (1986) ; T. Sjöstrand and M. Bengtsson, Computer Physics Commun. **43**, 367 (1987); T. Sjöstrand and M. Bengtsson, Computer Physics Commun. **46**, 43 (1987).

[41] F. Paige and S.D. Protopopescu, BNL Report No. 38034, 1986 (unpublished).

[42] F.A. Berends, W.T. Giele, H. Kuijf and B. Tausk, Nucl. Phys. **B357**, 32 (1991).

[43] J. Benlloch, Proceedings of the 1992 DPF Meeting, 10-14 Nov., 1992, Batavia, IL, ed. C.H. Albright *et al.,* World Scientific, (1993) p. 1091.

[44] F. Abe *et al.,* Phys. Rev. Lett. **79**, 4760 (1997).

[45] F. Ptohos (for the CDF Collaboration), Proceedings of the International Europhysics Conference on High Energy Physics 99, Tampere, Finland, July 17, 1999.

[46] J. Ohnemus and J. F. Owens, Phys. Rev. D **43**, 3626 (1991).

[47] T. Stelzer, Z. Sullivan and S. Willenbrock, Phys. Rev. D **58**, 3626 (1998); T. Stelzer, Z. Sullivan and S. Willenbrock, Phys. Rev. D **56**, 5919 (1997); T. Stelzer and S. Willenbrock, Phys. Rev. D **54**, 6696 (1996); T. Stelzer and S. Willenbrock, Phys. Lett. B **357**, 125 (1995).

[48] Raw jet energies are the observed values after performing the jet clustering, but prior to any corrections. The raw jet energies are used to select the data samples and are used in defining the four highest E_T jets.

[49] F. Abe *et al.,* Phys. Rev. D **47**, 4857 (1993).

[50] F. Abe *et al.,* Phys. Rev. Lett. **77**, 438 (1996).

[51] P. Bagnaia *et al.,* Phys. Lett. **144B**, 283 (1984).

[52] M. Lancaster, Proceedings of "Les Rencontres de Physique de la Vallée d'Aoste", La Thuile, March 1997, ed. M. Greco.

[53] MINUIT Reference Manual, CERN Program Library Entry **D506**, 1994.

[54] O. Dahl, T. Day, F. Solmitz and N. Gould, Lawrence Berkeley Lab, Alvarez Group Programming Note P-126 (1968).

[55] F. Abe *et al.,* Phys. Rev. Lett. **74**, 341 (1995).

[56] L. Orr, T. Stelzer, and W. J. Stirling, Phys. Rev. D **52**, 124 (1995); Phys. Lett. B **354**, 442 (1995).

[57] S. Bettelli, Ph.D. Thesis (unpublished), University of Pisa (1996).

[58] N. Eddy, Ph.D. Thesis (unpublished), University of Michigan (1998).

[59] G. Altarelli and G. Parisi, Nucl. Phys. **B126**, 298 (1977); Yu L. Dokshitzer, Sov. Phys. JETP **46**, 641 (1977); V. N. Gribov and L. N. Lipatov, Sov. J. Nucl. Phys. **15**, 438 (1972).

[60] H. L. Lai *et al.,* Phys. Rev. D **55**, 1280 (1997).

[61] F. Abe *et al.,* Phys. Rev. D **50**, 5562 (1994).

[62] F. Abe *et al.,* Phys. Rev. Lett. **82**, 271 (1999); Erratum *ibid.* **82**, 2008E (1999).

[63] K. Kondo, J. Phys. Soc. Jpn. **57** 4126 (1988); *ibid.* **60**, 836 (1991).

[64] E. W. Varnes, Ph.D. Thesis (unpublished), University of California, Berkeley (1997).

[65] Particle Data Group, C. Caso *et al.,* Eur. Jour. Phys C **3**, 1 (1998), p. 173.

[66] B. Abbott *et al.,* Phys. Rev. D **60**, 052001 (1998).

[67] L. Demortier, R. Hall, R. Hughes, B. Klima, R. Roser and M. Strovink, Fermilab Report No. FERMILAB-TM-2084 (1999).

[68] M. Lanzoni, University of Pisa Thesis (unpublished) (1996).

[69] D. Buskulic *et al.,* Phys.Lett. B **313**, 535 (1992).

[70] F. Abe *et al.,* Phys. Rev. D **53**, 1051 (1996).

[71] D.Buskulic *et al.,* Phys. Lett. B **284**, 177 (1992); P.Abreu *et al.,* Phys. Lett. B **322**, 459 (1994); R.Akers *et al.,* Phys. Lett. B **327**, 411 (1994).

[72] Monte Carlo studies showed that the jet probability distributions for light quark and gluon jets were similar, so that a single non-b probability distribution was used.

[73] S. Aota, Ph.D. Thesis (unpublished), University of Tsukuba (1997).